Version of Record: https://www.sciencedirect.com/science/article/pii/S0040603123002186
Manuscript_f7e7e28098e34118c95f0e1e804a8eb3

Temperature Corrections for Coaxial Cylindrical Viscosity Measurement Method on Molten Salt

Kent P. Detrick[a], Nicholas Jones[a], John Detrick[b], Joseph Talley[a], Tyler Green[a], Matthew Memmott[a*]

[a] *Chemical Engineering Department, Brigham Young University, Provo, UT, U. S. A.*

[b] *San Juan College 4601 College Boulevard Farmington, NM 87402*

*Corresponding Author.

Email address: memmott@byu.edu (Matthew Memmott)

Abstract

Modern industrial applications often require accurate measurements of high-temperature fluids such as molten salts. However, the commonly used coaxial cylindrical viscosity measurement method has an intrinsic bias when the calibration fluid and test fluid are run at significantly different temperatures due to the thermal expansion of solid container materials. In this study, we take a novel approach by deriving and quantifying the thermal expansion bias, β, for various common container materials using fluid dynamics arguments, thermal expansion data, and empirical methods. This work represents the first quantification of the thermal expansion bias and fills a significant gap in the current understanding. To validate our findings, we conducted an experiment on solar salt and applied the derived thermal expansion correction to the results, comparing them to independent studies. The results highlight the importance of the thermal expansion correction, which increases with rising temperature, particularly in high thermal expansion materials such as stainless steel, which has a bias of ~6% at 1000°C. Our contribution provides valuable insights into the accurate measurement of high-temperature fluids and offers a substantial advancement in addressing the thermal expansion bias, setting a new standard for future research in this field.

Key Words: Solar Salt; Couette Viscosity; Molten Salt; High-Temperature; Thermal Expansion Correction

1 Introduction

Molten salts are a group of high-temperature ionic fluids with use as a thermal energy storage medium, working fluids in heat transfer systems, and liquid nuclear power fuel [1]. Some solar power designs already make use of molten nitrate salts as thermal energy storage [2-4]. Most molten salts have low vapor pressure at high-temperatures (greater than 700°C) which thermodynamically improves efficiencies in heat pump cycles without the need for high pressure containment [5, 6]. Liquid fuel nuclear reactor concepts combine favorable liquid coolant properties with nuclear fuel solubility to improve fuel efficiency and safety [7-9].

Current methods for measuring molten salt viscosity include capillary, plumet, rotational, and oscillation techniques. A large body of data and measurement methods was compiled by Janz et al. [10-12] who recommended the oscillation technique for viscosity measurement due to the prevalence of low viscosities (less than 1cP) in most molten salts. However, rotational methods were initially better suited for high viscosity ranges such as in glasses and slags [12]. Recent advancements improve rotational methods to work in the molten salt viscosity range. Jin et al. noted limitations with the capillary and oscillation methods and recommended rotational methods for molten salts: oscillation methods require more experimental time, complicated calculations, and have a limited operation range (0.5 – 10 cP) compared to the rotational (0.1 – 10^6 cP) technique [13].

Rotational measurements are viable for molten salts, but require one of two method changes to properly account for thermal expansion: (1) a reliable temperature correction to account for thermal expansion, or (2) a calibrating fluid that is compatible within the same temperature range as the molten salt. The rotation methods rely on specific geometries replicated between a calibration fluid and the sample, and these problems directly influence the solid geometries influencing the measurements.

The main focus of this paper is to propose a thermal expansion correction method for the rotational viscosity measurement of high-temperature fluids, calculate the expected magnitude of this systematic error, or bias, as a function of temperature and container material, and perform an uncertainty propagation analysis on the correction. These new methods will allow for simultaneous room-temperature calibration and high-temperature viscosity measurement that removes the bias caused by thermal expansion in this scenario. This paper will first explain the theory behind the rotational method and then demonstrate the need for a temperature correction, propose an empirical correction method (along with an uncertainty propagation analysis), and measure the viscosity of solar salt ($NaNO_3$ – KNO_3, 60 – 40 wt%, 64.08 – 35.92 mol%) using the correction for demonstration purposes.

2 Materials and Methods

2.1 Theory

This section is broken into two subsections. The first section presents a physical model of fluid flow based on momentum transfer and fluid dynamics. From this model, the relationship between rotation, torque, and viscosity with the geometries of the system is derived. The next section discusses the high-temperature error problem, which arises from performing a calibration at a significantly different temperature than the measurement.

2.1.1 Coaxial Cylindrical Rotational Method

Bird et al. derived the viscosity expressions for the coaxial cylinder rotational viscosity measurement method in which the outer cylinder rotates about the inner cylinder (see Figure 1) [14]. A similar derivation was included in this section (only an outer cylinder was taken to be stationary and an inner cylindroid-spindle rotated) to review the model and its limitations. This model heavily influences the thermal expansion correction empirical model derived in the results section.

Figure 1 displays the physical model that describes the experimental cylindrical rotation and fluid flow. Using momentum transport arguments, the viscosity, μ, is put in terms of the geometries of the coaxial cylinders and other variables of the system. The expression is derived below using cylindrical coordinates r, z, and θ with the following assumptions:

- There are no flow components in the z and r directions (laminar flow)
- $v_\theta = v_\theta(r)$, angular fluid velocity is only a function the radial position, r

- $P = P(r, z)$, the pressure is symmetric about the z-axis
- The fluid is incompressible with uniform physical properties
- The fluid is Newtonian
- The model only accounts for the flow in the region bound by the distance L, and does not account for the tapered ends of the inner cylindroid-spindle (see Figure 1).

where v_θ is the viscosity in the rotational direction about the z – axis and P is the fluid pressure.

$$r - component \qquad -\rho_l \frac{v_\theta^2}{r} = -\frac{\partial P}{\partial r} \tag{1}$$

$$\theta - component \qquad 0 = \frac{d}{dr}\left(\frac{1}{r}\frac{d}{dr}(r v_\theta)\right) \tag{2}$$

$$z - component \qquad \frac{\partial P}{\partial z} = -\rho_l g \tag{3}$$

Where ρ_l is the fluid density and g is the acceleration due to gravity. Equation (1) describes the centrifugal force, equation (2) describes the liquid flow around the z – axis, and equation (3) describes the hydrostatic pressure in the fluid. Equation (2) is a differential equation solved by integration.

$$v_\theta(r) = \frac{C_1}{2} r + C_2 \frac{1}{r} \tag{4}$$

Where C_1 and C_2 are constants of integration generated by solving the differential equation.

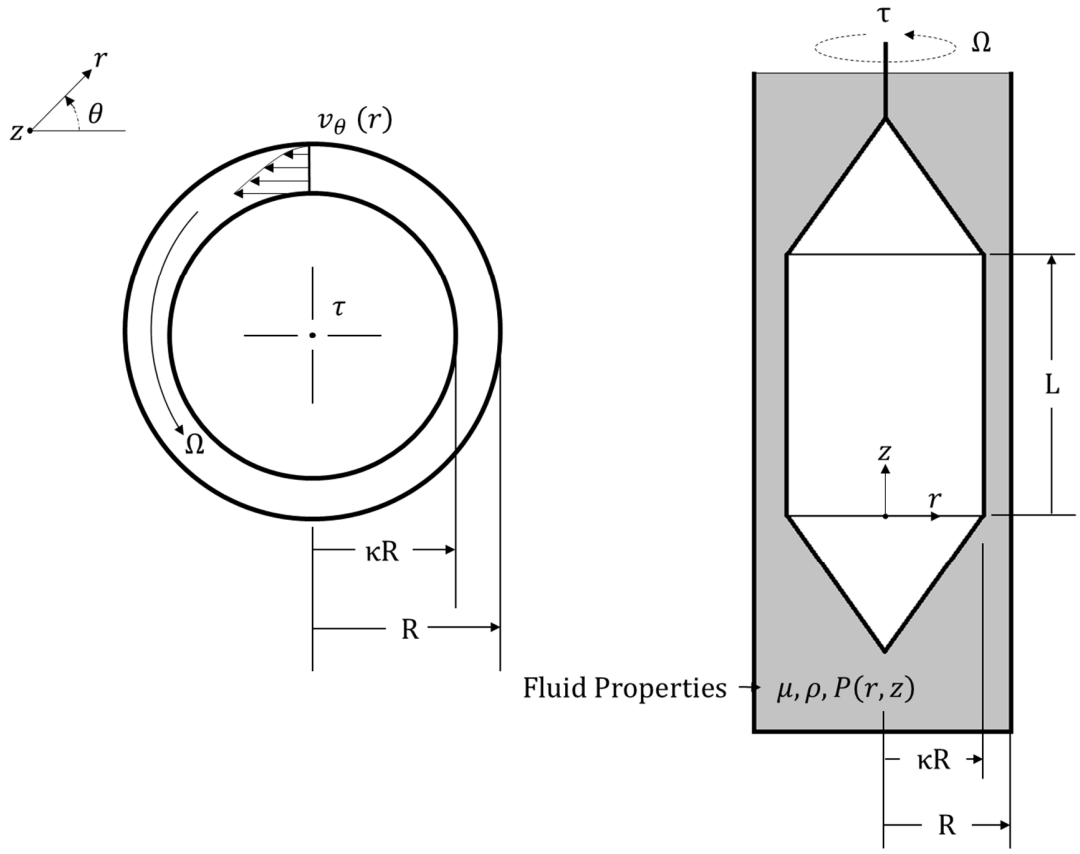

Figure 1: Graphical models of the coaxial cylinder rotation viscometer experiment in cylindrical coordinates. (left) Top-down view of two coaxial cylinders. (Right) Cut-away profile of the coaxial cylinders. The conical ends of the spindle (inner-cylinder) are assumed to have a negligible effect on the torsion, τ, experienced by the spindle rod.

Imposing the following boundary conditions (B.C.) resolves the constants of integration and yields equation (5).

B.C. 1: $v_\theta(\kappa R) = \Omega\kappa R$

B.C. 2: $v_\theta(R) = 0$

$$v_\theta(r) = \frac{\Omega\kappa R}{\left(\kappa - \frac{1}{\kappa}\right)}\left(\frac{r}{R} - \frac{R}{r}\right) \tag{5}$$

Where Ω is the rotation rate of the spindle, R is the radius of the cup cylindrical cavity and κ is the factor that when multiplied by R gives the radius of the spindle. Equation (5) gives the velocity profile. Using Newton's law of viscosity, the viscosity relates to the shearing force per unit area as in equation (6).

$$\tau_{r\theta} = -\mu r \frac{d}{dr}\left(\frac{v_\theta}{r}\right) = -2\mu\Omega\left(\frac{R}{r}\right)^2\left(\frac{\kappa^2}{1-\kappa^2}\right) \tag{6}$$

Where $\tau_{r\theta}$ is the momentum flux force in the θ direction on a unit area perpendicular to the r direction, and μ is the viscosity of the fluid. Equation (7) applies the shear force, T_z, calculated in equation (6) to the cylindrical surface of the spindle, ignoring the tapered ends (a.k.a. end effects), and factors in the lever arm for the torque to calculate the total force on the spindle supporting shaft caused by the sustained rotational motion. Where L is the effective length of the spindle.

$$T_z = (-\tau_{r\theta})\big|_{r=\kappa R} \bullet 2\pi\kappa RL \bullet \kappa R = 4\pi\mu\Omega LR^2\left(\frac{\kappa^2}{1-\kappa^2}\right) \tag{7}$$

For a long cylinder and $\kappa \approx 1$, equation (7) describes the main resistive force to a spindle rotating in a concentric cylinder filled with a Newtonian fluid.

Bird et al. makes an important note about the flow pattern described in this derivation. Equation (5) only represent one potential solution to this problem. In fact, under a different set of assumptions, mainly $v_r \neq 0, v_z \neq 0$, other flow patterns can persist in the form of "Taylor vortices" and even "doubly periodic flow" [14]. The three different laminar flow patterns persist under certain conditions dependent on the fluid properties, geometries of the system, and rotation speed. Above a critical rotation speed, a given fluid will predictably form "Taylor vortices," therefore, experimental results using the above derivation resulting in equation (7) will only be valid in the region below the critical rotation speed, Ω_{crit}. Equation (8) gives an empirical estimate for Ω_{crit} [14].

$$\Omega_{crit} = 41.3\left(\frac{\mu}{\rho_l\, R^2(1-\kappa)^{3/2}}\right);\ for\ \kappa \approx 1 \tag{8}$$

Calculating viscosity from equation (7) is possible, but often results in significant error due to the assumption that the flow of the fluid at the end of the spindle imparts no resistive force, that is, $\delta_{ef} \approx 0$. To account for the end effects in the system, viscosity standards with known viscosity and fluid dynamic properties similar to the test fluid can be employed [15]. At the limit where the test and calibration systems have identical properties, the two systems have a linear relationship. The end effects can be combined into a proportionality constant called the calibration constant, C, as expressed in equation (9).

$$T_z = 4\pi\mu\Omega LR^2\left(\frac{\kappa^2}{1-\kappa^2}\right) + \delta_{ef}(\mu, \Omega, L, R, \kappa) = C\mu\Omega \tag{9}$$

While this simplification is common practice for employers of the method, it has limitations. If the calibration fluid does not have similar physical properties to the test fluid, and/or if the system geometries change between the test and calibration systems, then the simplification can lead to significant errors because the linear relationship does not hold for large deviations between system properties (i.e. $\Delta\mu, \Delta\Omega, \Delta L, \Delta R, \Delta\kappa$).

To determine the value of the calibration constant, C, for a certain system, first measure T_z and Ω on a fluid of known viscosity. Then simply measure the torque, T_z, and rotation speed, Ω, for the same system, only substitute the calibration fluid with the fluid of interest. If the viscosity of the fluid of interest and the calibration fluid are similar, then the C calculated for the calibration fluid will be very close to the C for the system with the fluid of interest. By rearranging equation (9), the viscosity or the representative calibration constant for the system can be calculated with a correction for some end effect behavior (equations (10 a and b)).

$$\mu = \frac{T_z}{C\Omega} \tag{10 a}$$

$$C = \frac{T_z}{\mu\Omega} \tag{10 b}$$

In other words, the calibration constant, C, simplifies the real system by assuming a linear relationship between a calibration system and a test system. However, again, the linear assumption is only accurate so long as the calibration system (fluid and geometry) are nearly identical to the test system.

2.1.2 Thermal Expansion Bias

The previous section derives an equation modeling the relationship between torque, rotation speed, viscosity, and system geometries(equation (9)). However, the derivation assumes the geometries between the calibration system and the test system are nearly identical. This assumption does not hold for high-temperature measurements due to thermal expansion and temperature differences between the calibration system and the test system.

This theoretical derivation assists in anticipating the problems associated with high-temperature differences between a calibration sample and the test sample, but it is not intuitive what effect this will have on the viscosity measurement. In the physical system where all solids are the same material, as the temperature increases, the cup and spindle increase in volume in the R and L dimensions. Meanwhile, the gap between cylinders, $R - \kappa R$, remains constant. This leads to an increase in the surface area of the solid surface exposed to the fluid without changing the distance between the cup and spindle. The resulting expanded solid surface allows for the fluid to impart more shear force keeping all other variables constant, thereby artificially increasing the apparent viscosity in proportion to the recorded force. In other words, using a room temperature derived calibration constant on a high-temperature sample calculation systematically increases the measured viscosity.

There are three separate solutions to correcting this problem: (1) Perform the calibration and test at the same temperature, (2) apply a correction to adjust for thermal expansion effects on the calibration constant, and (3) assume that the error introduced by thermal expansion is negligible.

The implementation of the first method, (1), is currently hindered by a practical barrier: there is a lack of commercially available standard materials that can be used for calibration at high-temperatures for molten salts. Although some viscosities of molten salts have been measured and documented [10-12, 16], their use as standards is limited due to measurement errors and the lack of verification by multiple sources. Furthermore, these documented materials may not have sufficiently similar properties to the test fluid to be used as standards.

As for solutions (2) and (3), no proposals have been put forward for a method to correct the calibration constant. Additionally, it is unclear whether others have taken into consideration the potential impact of thermal expansion on the system, as researchers have simply assumed that its effect is negligible and accepted the associated error. However, it is possible that the consideration of this factor was missed during the transition of these techniques from room temperature systems to higher temperature systems.

2.2 Proposed Calibration Correction

This section proposes a method for correcting the error due to a temperature difference between the calibration and the sample systems. The correction must adjust the calibration constant so it more closely resembles the test sample system and remove thermal expansion bias:

$$C_{calibration} \overset{correction}{\Rightarrow} C_{adjusted} \approx C_{sample}$$

2.2.1 Ideal Case

In the ideal scenario, the calibration system exactly matches the high-temperature sample system:

$$C_{calibration} = C_{sample}$$

In order for these systems to be identical either the calibration is performed at the same temperature as the test sample, or the measurement requires two cup and spindle sets, the test sample cup and a calibration fluid cup that has been machined to exactly match the test sample cup under the test conditions except at room temperature. In this case no temperature correction is needed because there is no geometric difference between the two systems. Establishing this system is not practical however, because there are an infinite number of sample systems corresponding to each different system temperature, as the geometry of the system is a function of temperature.

$$C_{calibration}(\mathrm{T}_1) = C_{sample}(\mathrm{T}_2)$$

At each new T_2, high-temperature, a new geometry calibration cylinder must be precision machined to exactly fit the new dimensions of the sample system.

2.2.2 Empirical Correction

An alternative to the ideal case scenario, the empirical correction method, data is collected on different system geometries at room temperature and a model is created for thermal expansion changes in order to correct for geometric differences calculated for the higher temperature system. Calibration geometries provide data analogous to the test system and the empirical model effectively encompasses the varying geometries present in the test system. This empirical model can generate thermal expansion corrections for high-temperature test systems as long as the test system geometries resemble those used in the data for the calibration model's construction. The main benefit of this method over the ideal case being the use of an empirical model that bridges the gaps between data points, allowing for effective interpolation. This section outlines the process involved.

If G is a set of all the possible geometries that exist in the test system (the system of interest, i.e. solar salt liquidous temperature range) for the full range of temperatures, data for the empirical model should be collected such that $g \in G$, where g is a smaller set of geometries representative of G. The smaller set of geometries, g, should be representative of G in the sense that the data generated at each element of g will allow for interpolation for conditions which exist in the test system, but do not necessarily exactly match any one element of the subset g. In other words, the elements of g bound the elements of G and capture the form of the surface of interpolation, a representative sample.

The empirical model follows the form of equation (11) which was derived using equation (9) assuming δ_{ef} is close to zero. The first term is the main effect and the second term is the total end effect. The empirical model should follow this form to maintain its root in reality as opposed to taking the form of a high order polynomial.

$$C = 4\pi \mathrm{LR}^2 \left(\frac{\kappa^2}{1-\kappa^2}\right) + \delta_{ef}(\mathrm{R}, \mathrm{L}, \kappa, \mu, \Omega) \tag{11}$$

It is important to notice that the calibration variable, C, in equation (11) depends on three different system geometries, $C = C(\mathrm{R}, \kappa, \mathrm{L})$. If the two concentric cylinders are the same material, then κ is not a function of temperature, $\kappa \neq \kappa(\mathrm{T})$, because the inner and outer cylinder will thermally expand proportionally. The calibration variable will only be a function of R and L in this case. The empirical relationship between C and the variables R and L can take on a few different forms because the dependence of δ_{ef} on the geometries is unknown and varies with the shape of the cylinder ends. The main effect term, the first term in equation (11), has a second order relationship with R and a first order relationship with L. Therefore, the empirical model should contain a similar term. Equation (12) represents an empirical model that contains the main effect, $a_0 \mathrm{LR}^2$, as well as three other terms that approximate the relationship between the system geometry and the end effects.

$$C(\mathrm{R}, \mathrm{L}) = a_0 \mathrm{LR}^2 + \sum_{i=1}^{N} a_i \mathrm{L}^{m_i}\, \mathrm{R}^{n_i} \tag{12}$$

Where each a_i, $i = 0, 1, 2, \ldots, N$, is an adjustable parameter to make the best fit to the empirical data gathered, N is the number of terms in the equation less one, and m_i and n_i are exponents used to adjust the order of the relationship with C. Equation (12) sets the first term, $a_0 \mathrm{LR}^2$, to closely approximate the main effect derived in equation (11). The second term in equation (12) represents any other term that improves the fit of the model to the data (without over-fitting) by accounting for the end-effect changes due to a change in L and R.

The empirical approach offers the advantage of associating test system geometries with the corresponding calibration constant without the need to measure C at the exact test system geometry. This eliminates the need for an infinite number of systems to exactly match the experimental conditions, surpassing the limitations of the ideal case scenario. However, this method requires generating data from multiple tests at different geometries, significantly increasing the number of tests required for calibration from the, historically, single test performed at room temperature. The data needed to fit the model require different geometries and precision-machined cylinders, thus augmenting the cost and complexity of the experiment. Nonetheless, simplifying the empirical correction to encompass just the main effect reduces the cost and complexity while still accounting for significant thermal expansion effects.

The single term empirical model takes the form of equation (13), and minimizes the amount of data required to calculate the parameters to a single point. Equation (13) effectively separates the L and R dependence from the calibration constant where in previous methods it was assumed constant and lumped together into one variable.

$$C(\mathrm{R}, \mathrm{L}) = a_0 \mathrm{LR}^2 \tag{13}$$

Equation (14) is derived by substituting the single term empirical model for the calibration constant into equation (10 a).

$$\mu = \frac{T_z}{a_0 \mathrm{L} \mathrm{R}^2 \Omega} \tag{14}$$

Equation (14) gives the benefit over using equation (10 a) by allowing for the viscosity to be a function of the both L and R while still giving the same benefits of adjusting for some end effects due to it's roots in empirical data. Both L and R are a function of temperature and can be adjusted if the thermal expansion of the cup and spindle materials are well defined. Equation (14) can be further simplified by separating the thermal expansion length changes from the L and R variables and combining them into a single term using the linear thermal expansion ratio, $\frac{\delta_l}{l_{20°C}}$, as seen in equations (15 a-c).

$$\mu = \frac{T_z}{a_0 (\mathrm{L}_{20°\mathrm{C}} + \delta_\mathrm{L})(\mathrm{R}_{20°\mathrm{C}} + \delta_\mathrm{R})^2 \Omega} \tag{15 a}$$

$$\mu = \frac{T_z}{a_0 \mathrm{L}_{20°\mathrm{C}} (\mathrm{R}_{20°\mathrm{C}})^2 \left(1 + \frac{\delta_\mathrm{L}}{\mathrm{L}_{20°\mathrm{C}}}\right)\left(1 + \frac{\delta_\mathrm{R}}{\mathrm{R}_{20°\mathrm{C}}}\right)^2 \Omega} \tag{15 b}$$

$$\mu = \frac{T_z}{a_0 \mathrm{L}_{20°\mathrm{C}} (\mathrm{R}_{20°\mathrm{C}})^2 \left(1 + \frac{\delta_l}{l_{20°C}}\right)^3 \Omega} \tag{15 c}$$

Where $\mathrm{L}_{20°\mathrm{C}}$ and $\mathrm{R}_{20°\mathrm{C}}$ are the dimension of the spindle and cup from Figure 1 at room temperature. Under the conditions of the single term empirical model, it is clear from equation (15 c) that the parameter a_0 as well as the L and R values can be measured at room temperature. In fact, because each term a_0, $\mathrm{L}_{20°\mathrm{C}}$, and $\mathrm{R}_{20°\mathrm{C}}$ are all constants they can be recombined into a single calibration constant measured at room temperature, $C_{20°C}$, as seen in equation (16). Moreover, the thermal expansion terms can be combined because the relative thermal expansion of R and L are equivalent.

$$\mu = \frac{T_z}{C_{20°C} \beta \Omega}; \; \beta = \left(1 + \frac{\delta_l}{l_{20°C}}\right)^3 \tag{16}$$

Additionally, the thermal expansion component has been combined into a single term, β, to simplify the expression. Equation (16) is the general single-term empirical-model thermal expansion correction equation. This model applies to all materials and temperatures so long as the spindle and cup are the same material baring any other effect not accounted for in this derivation such as physical and chemical stability in the temperature range. The model does account for some degree of end effects because the model is based on empirical data (i.e. calculating $C_{20°C}$ from a room temperature standard solution), but the thermal expansion correction term, β, does not account for the temperature dependence of the end effects. The temperature dependence of the end effects is assumed to be insignificant compared to the main effect temperature dependence, but if this assumption does not hold for a certain system of interest then the reader is referred to the more complex empirical model, equation (12) .

2.3 Error Propagation Methods

In this discussion on error, it is important to note that certain terminology is used with specificity and distinction. Particularly, we refer to the thermal expansion correction as β, which is a correction factor

used to adjust viscosity calculations for changes in geometry due to thermal expansion and differences in temperature between the calibration and test fluid systems. Error propagation terminology is used to discuss the uncertainty in each measurement, and how these errors propagate through the viscosity calculation to influence the final measurement's accuracy. Uncertainties, therefore, refer to the random error in the individual measurements, and provide a statistic that represents the accuracy of the measurement. Finally, the mean confidence intervals for the predicted values of the model measure the spread of the calculated viscosity measurement data. In other words, the confidence intervals for the predicted values of the model measure the method's precision, rather than its accuracy.

The final viscosity measurement uncertainty is influenced by the thermal expansion correction. The error propagation for this situation can be estimated using several different methods [17]. All numerical values associated with an interval of uncertainty represent the 95% confidence interval for the mean measured value. Here, the uncertainty propagation has been calculated using the general formula equation (17).

$$\Delta J(\boldsymbol{x}) = \sqrt{\sum_{i=0}^{n}\left[\left(\frac{\partial J}{\partial x_i}(\bar{x_\iota})\right)^2 {\Delta x_i}^2\right]} \tag{17}$$

Where J is the function that describes the system of interest, such as equation (16) which describes the relationship between the viscosity and the physical constrains of the coaxial rotational cylinders; $\boldsymbol{x}$ is the vector which contain all the measurable variables on which J depends as described by the function; x_i is single variable or element of the vector $\boldsymbol{x}$; Δx_i is the absolute error associated with the measurement of x_i; and $\frac{\partial J}{\partial x_i}(\bar{x_\iota})$ is the partial derivative of J with respect to x_i evaluated at the sample average, $\bar{x_\iota}$, of x_i. This function assumes that in the range of Δx_i, the response in J is very close to linear, which is a good approximation for small values of Δx_i. Additionally, this function does not include any covariance effects, and assumes all the components of $\boldsymbol{x}$ are independent.

The impact factor, equation (18), represent the impact of the error in component, i, to the propagation of uncertainty to the function J. The factor indicates which variable and associated uncertainty makes the largest impact on the uncertainty of the target measurement by weighting the total error in the component variable by the influence of that variable in the final measurement. For instance, variable i may have a high degree of uncertainty, but the impact on the measurement due to the relationship between i and J is very small, resulting in low error propagation.

$$[Impact\ Facor] = \frac{\left(\frac{\partial J}{\partial x_i}(\bar{x_\iota})\right)^2 {\Delta x_i}^2}{\sum_{i=0}^{n}\left[\left(\frac{\partial J}{\partial x_i}(\bar{x_\iota})\right)^2 {\Delta x_i}^2\right]} \tag{18}$$

Equation (17) was used to evaluate the uncertainty associated with the calibration constant (equation (10 b)) as well as the final viscosity measurement with the thermal expansion correction, equation (16). summarizes the results.

2.4 Experimental Methods

An experiment was conducted to support the proposed corrections for the rotational coaxial cylinder method using solar salt. Solar salt was chosen due to its significance in the energy sector and the availability of prior measurements of its viscosity by several other researchers [12, 13, 18]. The experiment was also intended to validate the setup for future work on high melting point molten salts. The procedure established in this paper will be useful for future research in this area.

The thermal expansion effects can appear small and easily overlooked. In this paper, the goal is to (1) propose a method for temperature correction that accounts for thermal expansion, (2) assess the magnitude of the thermal expansion bias as a function of temperature and container material and (3) account for the uncertainty such a correction imparts to the viscosity measurement, allowing for the use of room temperature calibration fluids and the adjustment of the calibration constant for the different geometries that will exist in the test system due to thermal expansion.

2.4.1 Sample Preparation

The solar salt samples were prepared from their components $NaNO_3$ and KNO_3. Fisher Chemical produced both component salts, sodium nitrate, $NaNO_3$, (purity – 99.7% metals analysis) and potassium nitrate, KNO_3, (purity – 99.4% metals analysis) (see table). A vacuum furnace dried the salts at 200°C and -25 inHg gauge for 24 hours. The salts cooled to room temperature in the furnace. The base salts were mixed to their mass ratios by weight ($NaNO_3$ – KNO_3, 60.00 – 40.00 wt%). The salt was mixed in a nitrile container and the container was stored in secondary container filled with desiccant.

Calibration fluid was purchased from Cannon Instrument Company, Type N2. This fluid has a viscosity of 1.984 mPa · s at 25 °C. The N2 viscosity is about the same viscosity as the salt at about 400°C, close to the midpoint temperature tested in this experiment.

Table 1: Sample provenance information.

Compound	Source	Metals Purity (%mass)	Purification Method
Sodium Nitrate, $NaNO_3$	Fisher Chemical	99.7%	Vacuum Furnace 200°C, -25 inHg for 24 hours
Potassium Nitrate, KNO_3	Fisher Chemical	99.4%	Vacuum Furnace 200°C, -25 inHg for 24 hours
Calibration Fluid, Type N2	Cannon Instruments Company	N/A	None

2.4.2 Equipment Design

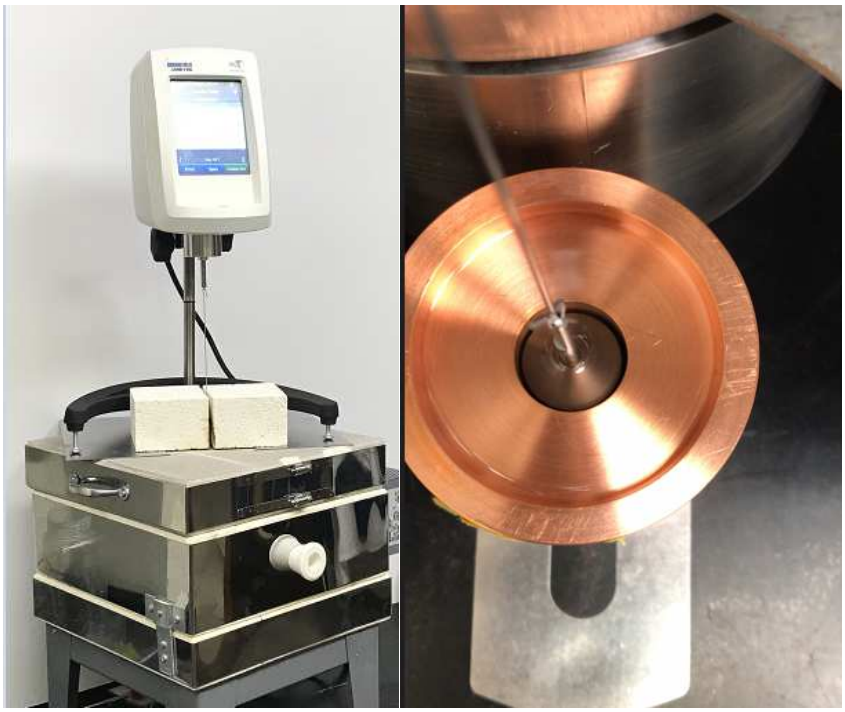

Figure 2: (Left) Viscometer (Brookfield Ametek DV2T) on top of furnace (Olympic Electric Kiln, HB84E) with the spindle extended down into the furnace. The furnace contains the cup, or outer cylinder. (Right) Outer cylinder (copper) with the spindle extended down into the cup. The cup was leveled with a stainless steel wedge. The setup was done without the furnace and with different colors for more visibility.

This experiment setup has two major pieces of equipment: the viscometer and the furnace. The viscometer is a Brookfield Ametek DV2T rotational viscometer and size SC4-18 stainless steel 316 spindle. The cup was made in house (see Figure 4) from stainless steel 316. The furnace is an Olympic Electric Kiln HB84E. Argonne National Laboratories previously used a similar setup [19], but the viscometer was held by a large stand, increasing the working distance between the furnace and the rheometer. They reported issues with alignment between the spindle and cup causing bias in measurement.

The spindle was aligned concentrically with the cup inside the furnace. A special procedure to align the cup with the spindle while the cylinder is inside the furnace was created for this study. The cup was placed in the furnace and leveled with stainless steel wedges and a digital level. A specially machined rod, which fit tightly in the cup well (0.0635 mm radial gap), was placed in the cup so the rod extended up and out of the furnace. The exposed end of the rod was threaded with 3/8 – 32 in. thread that fit onto the viscometer in place of the spindle (see Figure 3). After the viscometer and cup were aligned in this way, the aligning rod was removed and the spindle was attached. Still, small adjustments to the instrument alignment were required before each set of measurements to achieve the minimum viscosity.

Figure 3: A) Alignment rod inside viscometer cup. B) Alignment rod.

The experimental cup design is an improvement over a single shaft cylinder design, as it includes a novel feature that improves safety and accuracy (see Figure 4). The top of the cup features a shallow and wide 0.20 in. cut for an overflow cavity that is necessary because the liquid volume increases with temperature, and increased volume could lead to overflow (a potential safety hazard) and/or inconsistent measurements. The overflow cavity accommodates the extra liquid volume without significantly increasing the liquid level, which would increase the solid-liquid interface and sheer force on the rotating spindle, resulting in higher than true viscosity measurements. The wide 2.50 in. diameter of the cup increases its weight, which helps reduce measurement errors due to vibrations from the rotating cylinder or other sources and prevents the cup from tipping or spilling. However, the increased mass of the container material also increases the time for the test system to reach thermal equilibrium.

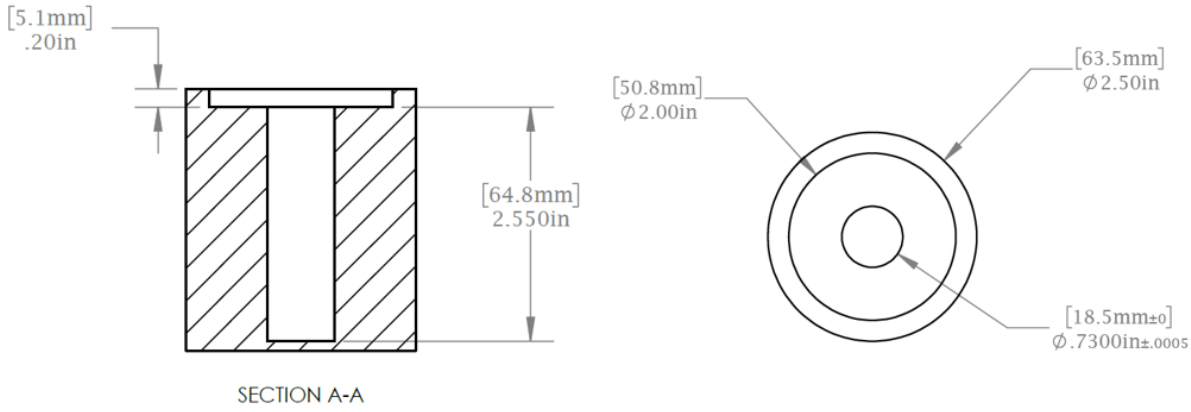

Figure 4: Cup dimensions for the outer cylinder and liquid container. (Left) a profile drawing of the cup cutaway showing the cavity depth and liquid overflow section. (Right) a top-down drawing of the cup indicating the dimension and tolerances of the outer cylinder and liquid overflow.

The furnace required one major modification. A 1 in. diameter port was added to the furnace lid which allowed the spindle to pass through the lid and into the cup. Additional firebrick was placed over the port during the tests to increase insulation and reduce the thermal gradient of the system.

The viscometer, cup, spindle and furnace details have been included in this section as well as the special alignment tool used to fix the spindle's orientation with the viscometer. The next section discusses the measurement procedure and operation of the equipment.

2.4.3 Experimental Procedure

The experimental procedure in this study consisted of two phases: calibration and test. During the calibration phase, the calibration constant was determined using the calibration fluid. The test phase involved measuring the viscosity of the solar salt. Although both phases followed the same basic procedure, the calibration was conducted entirely at room temperature, while the solar salt tests were performed at varying temperatures (above the melting point [12], 244°C, and below the decomposition temperature[20], 550°C). The setup and measurement procedures for both phases were detailed in this section.

A sample of calibration fluid or solid salt powder was placed in a level and aligned cup using a funnel with the furnace lid in place. The viscometer was level and aligned with the cup. The spindle was attached by a ridged wire hook and the viscometer was zeroed on air. The level spindle was inserted into the fluid by lowering the viscometer head using the metered stand until the spindle reached the bottom of the cup. The spindle was then raised back up by half a turn on the metered stand to ensure the spindles final position was centered in the cup with the spindle completely submerged in the fluid up to the reduced diameter portion of the shaft. The fluid was then tested on a set of Ω, spindle rotation rates, $\Omega = \{115, 120, 125, 130, 135, 140, 145, 150, 155, 160, 165, 170\}$ [rpm], in a randomized sequence. This range of Ω was set based on preliminary testing which established the limits for the system for the calibration oil (N2 Oil) and solar salt. At rotation rates less than 115 rpm the percent-of-maximum-torque on the measurement spring (torque%) measured less than 10%. The manufacturer of the viscometer indicates measurements of less than 10% torque% are not accurate. On the other end of the spectrum, at rotation rates greater than 170 rpm, the spindle rotation would not stabilize in an acceptable flow pattern required for the measurement. After the first set of Ω measurements were completed, the measurements were repeated with a different randomized sequence.

For solar salt measurements, there was an additional step required for the sample to reach thermal equilibrium. The system required 3 hours to reach thermal equilibrium after any change in system temperature. The set of temperatures measured,
$T = \{270, 300, 325, 350, 375, 400, 425, 450, 475, 500\}$ [°C], were also tested in a randomized sequence in duplicate, just as the rotation rates. The full set of rotation rates were tested at each temperature in duplicate.

A total of four samples on calibration fluid and three samples of solar salt were measured following these procedures (see Figure 6 and Figure 7).

In summary, the viscometer and cup were leveled and aligned. The furnace was set to a temperature and the system was allowed to reach thermal equilibrium. The viscosity was measured at a set of rotation rates in a random sequence. Finally, the calibration constant was calculated from the calibration fluid data and the solar salt viscosity was calculated from the calibration constant and measurement data for the test system.

3 Results

The results section of this paper is divided into three parts. First, we investigate the correction factor as a function of container material and temperature. We show that the correction factor is dependent on both the material of the container and the temperature of the experiment. Second, we quantify the total impact of the correction on the uncertainty of the viscosity measurement. The results show that the thermal expansion correction increases the accuracy of the viscosity measurement without unduly decreasing the precision. Last, we apply the correction to our experimental results and compare the results of the viscosity to those of the literature values. We carefully evaluate the difference between our methodology and that of the literature and demonstrate that the proposed correction significantly improves the accuracy of our results.

3.1 Material and Temperature Effects

Figure 5 shows the percent thermal expansion bias, $(\beta - 1) \times 100\%$, which demonstrates the trend of the correction factor as a function of temperature. The correction factor varies depending on the material, with the highest correction observed for stainless steel 316, while the lowest correction was observed for Graphite Grade 7087. The correction factor increases monotonically with temperature. The thermal expansion bias for common metallic container materials for molten salts for temperatures between 800 and 1000°C is estimated to be about 4-6%. The correction factor was calculated using the thermal expansion data provided by Touloukian et al. [21].

These data clearly show a significant bias due to thermal expansion especially for the transition metals (except Mo). While the end effects were not accounted for in the single term empirical model, the temperature dependance of the end effects would certainly further increase the thermal expansion bias at higher temperatures due to the same physical reasoning proposed earlier; the solid surface expands imparting more sheer force at the solid surface to the rotating spindle, including the spindle ends. Therefore, the total effect of the thermal expansion bias is likely higher than only using the β correction accounts for.

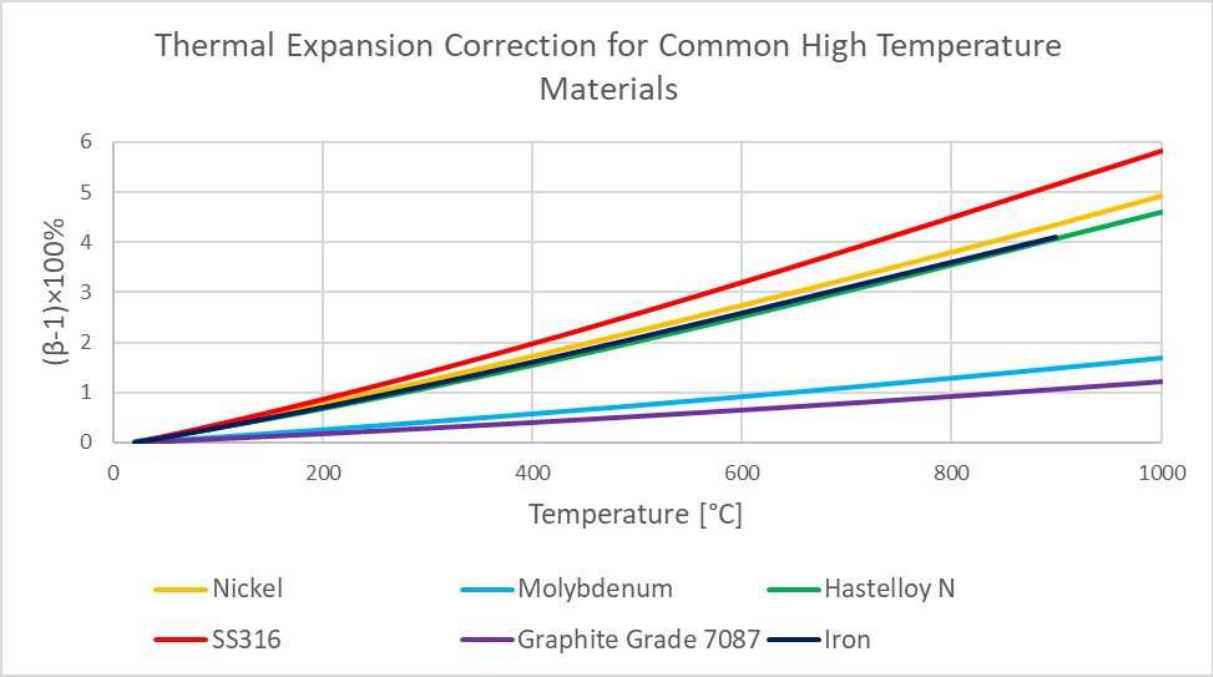

Figure 5: This y-axis indicates the percentage thermal expansion bias as a function of temperature for various materials.

3.2 Error Propagation

The calibration constant, $C_{20°C}$, component errors were provided by the manufacturer for the T_z, torque uncertainty, $\mu(T)$, standard N2 viscosity uncertainty and temperature dependence, Ω, rotation measurement uncertainty, and T, temperature measurement as measured by the viscometer's built-in thermocouple.

Table 2: The list of errors associated with the calibration constant calculation and an estimate of the total uncertainty associated with the calibration constant using equations (17) and (18).

$J = C_{20°C} = \frac{T_z}{\mu(T)\Omega}$	Units	$\bar{x}$	Δx	Expanded Relative Uncertainty, Ur	Impact Factor
$\mu_{Standard}$	[Pa · s]	0.002021	4E-06	0.21%	0.88%
Ω	[rad/s]	14.399	0.005	0.03%	0.02%
T_z	[N · m]	9.12E-06	9E-08	1.00%	19.86%
T	[K]	297.4	1.0	0.34%	79.24%
C	[m^3]	3.13E-04	7E-06	2.24%	

The uncertainty in the final viscosity measurement was calculated using the same methodology as with the calibration constant using equation (17), (results in Table 2). The results for the calibration constant were included in the final viscosity measurement error propagation. The Ω, rotation measurement uncertainty and the T_z, torque, uncertainty were provided by the manufacturer of the viscometer. The Temperature measurement, T, was taken with the thermocouple used to control the temperature of the furnace, and the uncertainty is the uncertainty typical of a Type-K thermocouple. The error associated with the β factor originates from the uncertainty in the thermal expansion measurements, and was calculated by generating a normally distributed random sample of possible β values given the uncertainty

in thermal expansion where the sample size is equal to 1×10^6. The base uncertainty in thermal expansion measurements was estimated at less than 4% by the source [21].

Table 3: The list of errors associated with the viscosity measurement and an estimate of the total uncertainty associated with the viscosity using equations (17) and (18).

$J = \mu = \frac{T_z}{C_{20°C}\beta(T)\Omega}$	Units	$\bar{x}$	Δx	Expanded Relative Uncertainty, Ur	Impact Factor
$C_{20°C}$	$[m^3]$	3.13E-04	7E-06	2.24%	83.11%
Ω	$[rad/s]$	15.137	0.005	0.034%	0.02%
T_z	$[N \cdot m]$	1.12E-05	1.1E-07	1.00%	16.51%
T	[K]	660.2	2.2	0.33%	0.003%
β	[]	1.0190	0.0015	0.15%	0.36%
μ	$[Pa \cdot s]$	2.25E-03	6E-05	2.54%	

As seen by this analysis, the total uncertainty in the viscosity measurement is about 2.54%, and the thermal expansion correction uncertainty only contributes about 0.36% of that uncertainty, the majority of uncertainty propagating from the calibration constant. Further, the majority of the calibration constant uncertainty originates from the uncertainty in the calibration fluid temperature uncertainty. As a whole, the average β value in these experiment conditions accounts for a 1.9% bias while only increasing the overall uncertainty by less than 0.01% because it has a low relative error and a low impact factor.

Jin et al. performed a very similar experiment, using different materials. They used an unspecified graphite material for their cup and spindle, which have a very low thermal expansion correction (see Figure 5). In their error analysis, the total error amounted to 2.5% as well using a similar method. Their uncertainty analysis included the uncertainties in the T_z, Ω, standard oil viscosity, temperature, and $C_{calibration}$ measurements. They calculated that the combined effects of these uncertainties amounted to 2.5% relative error in the final viscosity measurements. Therefore, the error analysis has been confirmed for two independent systems, and this thermal expansion correction does not seem to greatly increase the overall uncertainty.

The bias due to thermal expansion will increase with increasing temperature. Additionally, a material with a higher thermal expansion coefficient will increase the bias. There are several molten salts which are candidate materials for use in industry that have operating conditions well above the highest stable temperature for solar salt, such as FLiBe (LiF – BeF_2, 66.67 – 33.33 mol%, melting point – 459°C), FLiNaK (LiF – NaF – KF, 46.5-11.5-42 mol %, melting point – 454°C), and NaF-ZrF_4 mixtures (melting points – 500-750°C), and the thermal expansion correction for this measurement method should be applied in each of these high-temperature cases for more accurate results.

3.3 Viscosity Measurements

The viscosity measurements for this work are plotted against the three other viscosity measurements in Figure 6. Janz et al. and Zavoico have a lower viscosity reported in the higher temperature range than was reported by this work and especially lower than those results reported by Jin et al. At the lower temperature range Zavoico reports the highest viscosity. Zavoico did not report their methodology, so it is difficult to surmised a reason for this behavior. Jin et al. reported results that were not corrected for temperature. However, the graphite used for the cup and spindle material presumably has a low thermal expansion correction factor. The higher viscosity they reported in the high-temperature range aligns with

the expected error caused by the temperature difference between the calibration and test samples. Nevertheless, without additional information regarding the thermal expansion coefficient of their container material, it is not possible to quantify the causality between the temperature error and the increased viscosity at higher temperatures.

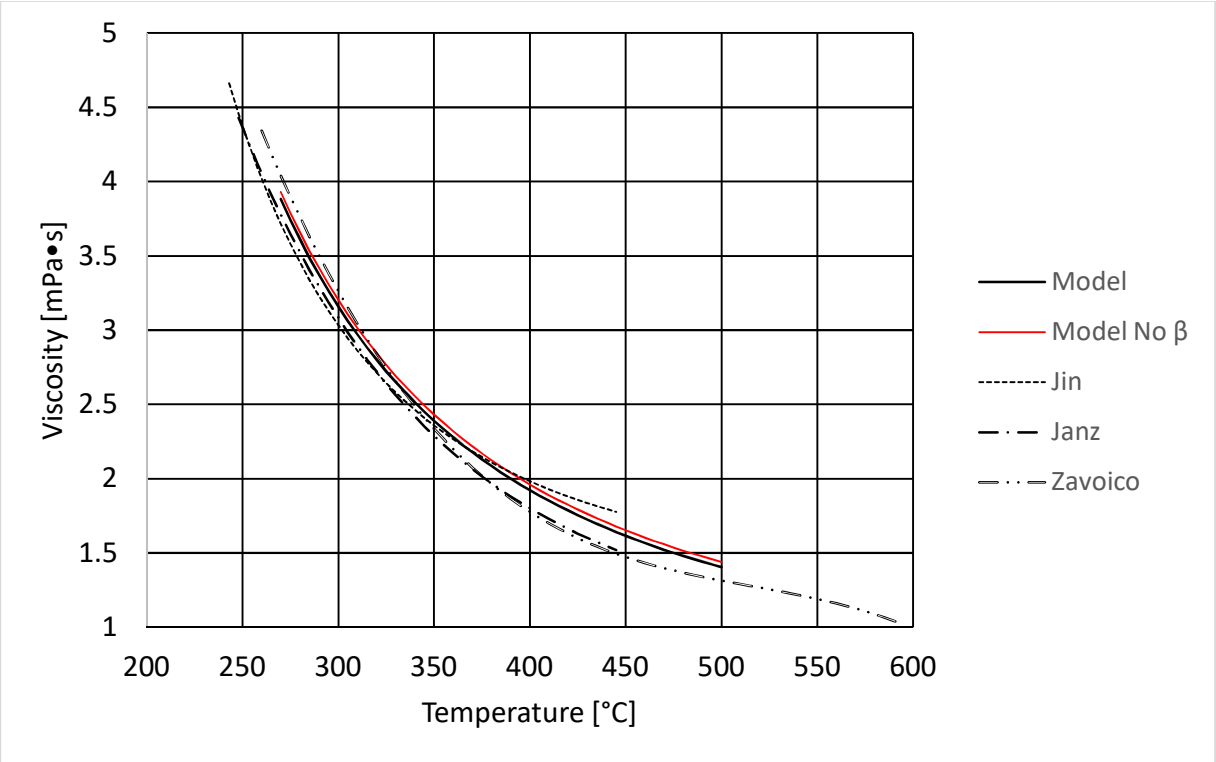

Figure 6: Solar salt viscosity measurements from this work and the literature. Jin et al. [13] used the coaxial rotational method using graphite (no thermal expansion correction), and Janz et al. [12] reported values from the oscillation method. Zavoico [18] did not report their methodology. The Model and "Model No β" lines are from this work, the latter is based on the data without a thermal expansion correction for easier visualization of the correction magnitude.

These results suggest there are other sources of error in this measurement not accounted for as part of the previous analysis derived from the system geometries, fluid dynamics, and thermal expansion data. Other sources of error include the non-linear dependence of the calibration constant over the range of viscosity measurements, the uncertainty in salt composition, spindle and cup alignment variability, and the uncertainty in temperature as associated with the fundamental dependence of viscosity on temperature. Janz et al. has some composition data that could be used to estimate the dependence and error propagation of composition on viscosity. Using multiple calibration fluids for higher resolution over the full viscosity range of the experiment could help resolve some of the non-linear behavior of the calibration constant and its influence on the final measurement. Adjustments in experiment design could nearly eliminate the alignment problems as these measurements become more common and manufacturers develop experiment designs that are more compatible with molten salts. The intrinsic dependence of viscosity on temperature generally decreases non-linearly as temperature increases, and several models have been used to estimate the non-linear behavior [22]. Generally the viscosity changes exponentially with temperature changes, so the degree of uncertainty in the temperature measurement has the largest contribution to the uncertainty in the final viscosity measurement (see Table 1). Increasing the accuracy of the temperature measurements in the salt and in the calibration fluid will greatly reduce the uncertainty of the final

viscosity measurement. Experiment designs that account for this error should focus on implementing more accurate thermocouples compatible with high-temperatures and reducing thermal gradients in the furnace with high quality insulation and heating element distribution. However, the scope of this paper is solely to address and propose a method for the thermal expansion bias associated with this measurement method. Further effort on these other method improvements is reserved for future work.

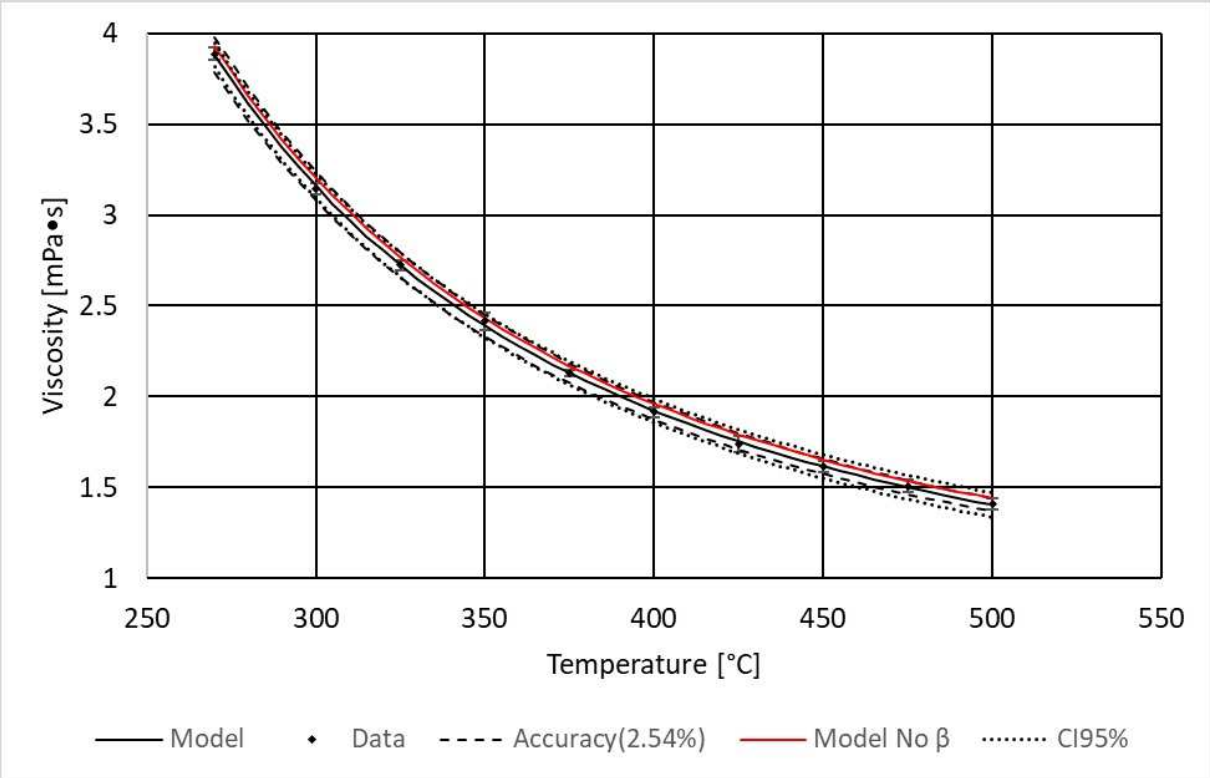

Figure 7: The model for the relationship between temperature and viscosity of solar salt, equation (19). The data was plotted here with error bars associated with the standard deviation of the three samples at each sample at each temperature. The calculated accuracy from Table 2 was represented by the area between the dashed lines. The red line labeled "Model No β" was the model without the correction due to thermal expansion. The "CI95%" represents the 95% confidence interval for the predicted values of the model (with the thermal expansion correction).

Equation (19) is the model for viscosity of solar salt as a function of temperature. The parameters were calculated by minimizing the sum of the squared residuals. The three parameter model was chosen for the close fit to the data, and for comparability between the other existing models in the literature [12, 13, 18].

$$\mu[\mathrm{mPa}\cdot\mathrm{s}] = A\exp\left(\frac{B}{T[\mathrm{K}]}+\frac{C}{(T[\mathrm{K}])^2}\right) \tag{19}$$

Parameter	Value	Std. Error	Lower 95% CI	Upper 95% CI
A	0.563	0.131	0.295	0.832
B	-103	292	-702	496
C	6.25E+05	9.08E+04	4.39E+05	8.12E+05

Table 4: The relative and percent error over the test temperature range after applying the theoretical temperature correction a total of N=3 samples measured at each temperature. The expanded relative uncertainty for the viscosity measurements is estimated as 2.54% (see Table 3)

Temperature	Average Viscosity	Standard Deviation, N=3
[°C]	[mPa·s]	[mPa·s]
270	3.89	0.03
300	3.15	0.03
325	2.72	0.03
350	2.42	0.05
375	2.13	0.02
400	1.91	0.03
425	1.74	0.04
450	1.61	0.03
475	1.51	0.04
500	1.41	0.03

4 Conclusions

Our study highlights the challenges associated with using the rotational concentric cylinder viscosity measurement method for high-temperature molten salts. The dimensions of the solid surfaces used in the experiment are crucial to the fluid dynamic description of the system. The available calibration fluids are not suitable for high-temperature systems, and a measurement bias is introduced when the test fluid and calibration fluid are run at different temperatures and the solid material used in the test is sensitive to thermal expansion. While the intrinsic dependence of viscosity on fluid temperature and associated measurement errors contribute most significantly to the final viscosity error (2.54% relative error), the thermal expansion bias, β (bias of up to 6%)(see equation (16)) is still significant to improving the accuracy of the measurement. The method proposed for correcting for this error takes in the main effects of the geometry changes without significantly increasing the uncertainty (total uncertainty increase >0.06%) in the final measurement. Further work in improving the accuracy of this measurement should focus on improving the precision of the temperature measurements and reducing thermal gradients in the measurement system as this has the highest impact on the final viscosity measurement uncertainty. Additionally, values for the solar salt viscosity are reported in the viscosity range of 3.89 – 1.41 mPa·s at a temperature range of 270 – 500 °C.

Declaration of Competing Interest

The authors declare that they have no competing interests associated with this research project. There are no financial, personal, or professional relationships or affiliations that could be perceived as potential conflicts of interest.

CRediT Authorship Contribution Statement

Kent Detrick: Conceptualization, formal analysis, data curation, investigation, methodology, validation, writing – original draft, review & editing, project administration. **Nicholas Jones**: data curation, writing –

original draft, review & editing. **John Detrick**: Writing – review & editing. **Joseph Talley**: data curation, writing – review & editing, **Tyler Green**: data curation, writing – review & editing, **Matthew Memmott**: writing – review & editing, resources, supervision, funding acquisition.

Data Availability

Data will be made available on request.

Acknowledgements

This work was supported by the U.S. Department of Energy, Office of Nuclear Energy, Nuclear Energy University Program under Project 19e17413 (CID: DENE0008870).

Declaration of Generative AI and AI-assisted technologies in the writing process

During the preparation of this work the authors used GPT-3.5, developed by OpenAI, in order to improve readability and language. After using this tool/service, the authors reviewed and edited the content as needed and take full responsibility for the content of the publication.

Bibliography

1. Serp, J., et al., *The molten salt reactor (MSR) in generation IV: Overview and perspectives.* Progress in Nuclear Energy, 2014. **77**: p. 308-319.
2. Herrmann, U., M. Geyer, and D. Kearney. *Overview on thermal storage systems. Workshop on Thermal Storage for Trough Power Plants*. 2002 [cited 2019 30 September, 2019]; Available from: https://energiatalgud.ee/img_auth.php/f/ff/Herrmann%2C_U.%2C_Geyer%2C_M.%2C_Kearney%2C_D._FLABEG_Solar_Int._GmbH._Overview_of_thermal_storage_systems._2002.pdf.
3. Zhang, H., et al., *Thermal energy storage: Recent developments and practical aspects.* Progress in Energy and Combustion Science, 2016. **53**: p. 1-40.
4. *Largest solar thermal power stations (CSP) list*. 2023; Available from: https://list.solar/plants/largest-plants/csp/.
5. Jiang, D., et al., *Fluoride-salt-cooled high-temperature reactors: Review of historical milestones, research status, challenges, and outlook.* Renewable and Sustainable Energy Reviews, 2022. **161**: p. 112345.
6. Todreas, N.E. and M.S. Kazimi, *Nuclear Systems Volume 1 Thermal Hydraulic Fundamentals*. 2 ed. Vol. 1. 2011, Boca Raton, FL 33487-2742: CRC Press Taylor & Francis Group.
7. Hargraves, R. and R. Moir, *Liquid Fluoride Thorium Reactors: An old idea in nuclear power gets reexamined.* American Scientist, 2010. **98**(4): p. 304-313.
8. Abu-Khader, M.M., *Recent advances in nuclear power: A review.* Progress in Nuclear Energy, 2009. **51**(2): p. 225-235.
9. Roper, R., et al., *Molten salt for advanced energy applications: A review.* Annals of Nuclear Energy, 2022. **169**: p. 108924.
10. Janz, G.J., et al., *Molten salts: volume 4, Part 1, fluorides and mixtures electrical conductance, density, viscosity, and surface tension data.* Journal of Physical and Chemical Reference Data, 1974. **3**(1): p. 1-115.
11. Janz, G.J., et al., *Molten salts: Volume 4, part 2, chlorides and mixtures—electrical conductance, density, viscosity, and surface tension data.* Journal of Physical and Chemical Reference Data, 1975. **4**(4): p. 871-1178.

12. Janz, G.J., et al., *Molten Salts: Volume 3 Nitrates, Nitrites, and Mixtures: Electrical Conductance, Density, Viscosity, and Surface Tension Data.* Journal of Physical and Chemical Reference Data, 1972. **1**(3): p. 581-746.
13. Jin, Y., et al., *Accurate viscosity measurement of nitrates/nitrites salts for concentrated solar power.* Solar Energy, 2016. **137**: p. 385-392.
14. Bird, R.B., W.E. Stewart, and E.N. Lightfoot, *Transport Phenomena*. Second Edition ed. 2007, New York, NY: John-Wiley & Sons, Inc. . 905.
15. Lindsley, C.H. and E.K. Fischer, *End-Effect in Rotational Viscometers.* Journal of Applied Physics, 1947. **18**(11): p. 988-996.
16. Janz, G.J., *Molten Salts Handbook*. 1967: Academic Press Inc. (London) LTD.
17. Ku, H.H., *Notes on the use of propagation of error formulas.* Journal of Research of the National Bureau of Standards, 1966. **70**(4).
18. Zavoico, A.B., *Solar Power Tower Design Basis Document*. 2001, Sandia National Laboratories: Albubquerque, NM.
19. Rose, M.A., E. Wu, and M.A. Williamson, *Thermophysical Property Measurements: Improved Density, Viscosity and Thermal Diffusivity Methods*. 2020, Argonne National Lab.(ANL), Argonne, IL (United States).
20. Carling, R.W., et al., *Molten nitrate salt technology development status report*. 1981, ; Sandia National Lab. (SNL-CA), Livermore, CA (United States); Sandia National Lab. (SNL-NM), Albuquerque, NM (United States). p. Medium: ED.
21. Touloukian, Y.S., et al., *Thermal Expansion Metallic Elements and Alloys*. Thermophysical Properties of Matter The TPRC Data Series, ed. Y.S. Touloukian. Vol. 12. 1975, New York-Washington: IFI/Plenum Data Company, Plenum Publishing Corporation.
22. Viswanath, D.S., et al., *Viscosity of Liquids Theory, Estimation, Experiment, and Data*. 2007, https://doi-org.erl.lib.byu.edu/10.1007/978-1-4020-5482-2: Springer, Dordrecht.